Biosensors and Bioelectronics 271 (2025) 117048

Contents lists available at ScienceDirect

Biosensors and Bioelectronics

journal homepage: www.elsevier.com/locate/bios

Magnetophoretic slider assay for electrochemical detection of SARS-cov-2 nucleocapsid protein in nasal swab samples

Nutnaree Fukana [a,b,c], Joowon Park [c], Gilberto J. Silva Junior [c,d], Lauren E. Malsick [e], Emily N. Gallichotte [e], Gregory D. Ebel [e], Brian J. Geiss [e,f], David S. Dandy [f,g], Mauro Bertotti [d], Duangjai Nacapricha [a,b,**], Thaisa A. Baldo [c,***], Charles S. Henry [c,f,g,*]

[a] Department of Chemistry and Center of Excellence for Innovation in Chemistry, Faculty of Science, Mahidol University, Rama 6 Road, Bangkok, 10400, Thailand
[b] Flow Innovation-Research for Science and Technology Laboratories (Firstlabs), Thailand
[c] Department of Chemistry, Colorado State University, Fort Collins, CO 80523, USA
[d] Department of Fundamental Chemistry, Institute of Chemistry, University of São Paulo, Av. Professor Lineu Prestes, 748, 05513-970, São Paulo, SP, Brazil
[e] Department of Microbiology, Immunology and Pathology, Colorado State University, CO, USA, 80523
[f] School of Biomedical Engineering, Colorado State University, CO, USA, 80523
[g] Department of Chemical and Biological Engineering, Colorado State University, CO, USA, 80523

ARTICLE INFO

Keywords:
COVID-19
Electrochemical biosensors
Immunoassay
Magnetophoresis
Microfluidics
Diagnostic platform

ABSTRACT

The COVID-19 pandemic highlighted the need for rapid and sensitive diagnostic tools. In this work, the Magnetophoretic Slider Assay (MeSA) was integrated with electrochemical detection (eMeSA) using screen-printed carbon electrodes for the first time for the detection of SARS-CoV-2 nucleocapsid protein (NP). A sandwich enzyme-linked immunosorbent assay (ELISA) was performed on streptavidin-labeled magnetic beads (MBs). The streptavidin MB/biotinylated antibody/NP complexes were added into the sample inlet, where the beads were trapped using an external magnet while the solution rehydrated the HRP-labeled antibody (HRP-Ab) and 3,3′,5,5′-tetramethylbenzidine (TMB) pads. By sliding the external magnet along the channel, the bead complexes were moved to the reservoir under the HRP-Ab pad, forming sandwich complexes. These complexes were subsequently moved back across the device to reach the electrochemical detection zone, where they reacted with released TMB, which underwent oxidation upon reacting with HRP attached to the detection antibody, followed by reduction due to the voltage applied to the working electrode (0.0 V *vs.* Ag reference electrode). The assay showed promising results in detecting SARS-CoV-2 in 10 min, with a limit of detection of 8.89 ng/mL NP and 78.02 PFU/mL inactivated virus. The results from 15 human samples demonstrated 100% clinical specificity and 100% clinical sensitivity for samples with RT-PCR cycle threshold (C_t) values from 19 to 30, meeting WHO criteria for COVID-19 diagnostics. The eMeSA offers an alternative to traditional ELISA for a wide range of point-of-care and point-of-need diagnostic applications.

1. Introduction

Severe acute respiratory syndrome coronavirus 2 (SARS-CoV-2) is a coronavirus variant responsible for the coronavirus disease 2019 (COVID-19) pandemic (Bar-On et al., 2020; Fenwick et al., 2021; Wu et al., 2023). SARS-CoV-2 is primarily transmitted through respiratory droplets and affects human health by causing respiratory illnesses that can range from mild symptoms (*e.g.,* cough and fever) to severe conditions such as pneumonia (Afshari et al., 2021). Due to its high contagiousness, it has rapidly spread and caused more than 7 million deaths worldwide (data accessed on October 20, 2024) (WHO COVID). Given the ongoing increase in reported cases and the daily appearance of new infections, the development of decentralized and accessible diagnostic tools is imperative for facilitating disease detection and early

* Corresponding author. Department of Chemistry, Colorado State University, Fort Collins, CO 80523, USA.
** Corresponding author. Department of Chemistry and Center of Excellence for Innovation in Chemistry, Faculty of Science, Mahidol University, Rama 6 Road, Bangkok 10400, Thailand.
*** Corresponding author. Department of Chemistry, Colorado State University, Fort Collins, CO 80523, USA.
E-mail addresses: dnacapricha@gmail.com (D. Nacapricha), thaisabaldo@gmail.com (T.A. Baldo), chuck.henry@colostate.edu (C.S. Henry).

https://doi.org/10.1016/j.bios.2024.117048
Received 13 August 2024; Received in revised form 5 December 2024; Accepted 6 December 2024
Available online 7 December 2024

intervention (Giri et al., 2021; Abdelhamid and Badr, 2021). Currently, reverse transcription polymerase chain reaction (RT-PCR) is the most widely used method for clinical detection of SARS-CoV-2 due to its high sensitivity and specificity (Kudr et al., 2021; Ferreira et al., 2023). Although RT-PCR is used as the gold standard, it is labor-intensive, has complicated operating steps, and is time-consuming. As an alternative, enzyme-linked immunosorbent assays (ELISAs) have been used to detect biomarkers (antigens and antibodies) for COVID-19 (Ferreira et al., 2023; Perveen et al., 2023; Kilic et al., 2020). Traditional ELISA still requires a laboratory setting and skilled technicians, and the assay can take several hours to complete (Ong et al., 2020).

To address the needs of point-of-care (POC) testing, moving away from conventional bulky instruments and focusing on portable sensing devices is necessary. Lateral flow assays (LFAs) provide a rapid result but also have several significant limitations (Ferreira et al., 2023; Perveen et al., 2023; Kilic et al., 2020). With LFA, the sample is introduced to a sample pad and flows along the test strip *via* capillary action. As the sample flows, it encounters antibodies or antigens immobilized on different test lines, producing one colored line for negative and two lines for positive samples (Rad et al., 2023). These assays deliver rapid outcomes to end-users. Nevertheless, it is essential to note that traditional LFAs are limited in terms of sensitivity because one antigen binds one reporting particle (Liu et al., 2021).

Among the various portable sensors reported in the literature, electrochemical sensing devices stand out for being rapid and practical tools for POC diagnostics (Sankar et al., 2024; Akhavan et al., 2012; Kumar et al., 2022). Multiple efforts have been made to develop electrochemical biosensors to detect COVID-19 biomarkers (Kudr et al., 2021; Ferreira et al., 2023; Madhurantakam et al., 2022; Rocha et al., 2024; Rahman, 2022). For the assembly of these biosensors, the electrodes are commonly further modified with biological molecules (*e.g.,* nucleic acids (Naorungroj et al., 2023), antibodies (Rocha et al., 2024), enzymes (Ferreira et al., 2023; Sankar et al., 2024) and aptamers (Ferreira et al., 2023; Sankar et al., 2024)) to enhance the sensitivity and specificity of the detection. However, the electrode is not always modified with biomolecule, but instead, the recognition elements can be immobilized on a separate support, such as magnetic beads (MBs).

Magnetophoresis is the process of manipulating magnetic beads (MBs) within a magnetic field in a fluid. Beads or particles with magnetic properties (*e.g.,* magnetic, paramagnetic, or magnetic nanocomposites (Naghdi et al., 2022)) move to the desired position when exposed to a magnetic field gradient, enabling the separation and/or the concentration of the analyte of interest from sample matrix (Pamme and Manz, 2004). Moreover, this technique facilitates the removal of non-specifically bound substances through wash buffers, thereby enhancing assay sensitivity and specificity. Using MBs also leads to an increase in detection sensitivity, since the MBs can be loaded with more antibodies than a flat surface, preconcentrating the analyte before delivery to the electrode surface (Ferreira et al., 2023; Kudr et al., 2018; Paleček and Fojta, 2007). Therefore, MB-based electrochemical assays have been extensively developed to detect SARS-CoV-2 in various clinical samples (Fabiani et al., 2021, 2024; Malla et al., 2022, 2023; Cajigas et al., 2022; Durmus et al., 2022; Vásquez et al., 2022; Nascimento et al., 2022). Coupling these techniques with microfluidic systems is a potential alternative to automate and simplify immunoassays.

Microfluidic devices can readily handle small sample volumes with high accuracy and require no additional user steps, making them ideal for POC testing. The integration of magnetophoresis with microfluidics was first demonstrated by Pamme et al. using a PDMS and glass microfluidic system (Pamme and Manz, 2004). Although this approach simplifies laboratory procedures by enabling sequential reagent binding and washing during sample flow, the method requires an external pump to drive the flow, which limits its portability and user-friendliness for POC applications. Recently, the Henry Group published the first paper-based pump-free magnetophoretic device to overcome the need for an external pump with magnetophoresis (Call et al., 2020). This system allows the particles to flow *via* capillary action in a gap between stacked layers of paper and hydrophilic transparency film. Although this work successfully demonstrated a proof of concept for magnetophoretic microfluidic paper-based analytical devices (μPADs) for *E. coli* detection, the system is challenged by the fact that only a fraction of the conjugated magnetic beads passed through the device. Later, Call et al. proposed another approach to overcome this detection limitation using the Magnetophoretic Slider Assay (MeSA) device with colorimetric detection (Call et al., 2023). The device channel is created by stacking layers of alternating polyethylene terephthalate (PET) and double-sided adhesive films. The assay simplifies user operation based on the manipulation of magnetic particles by sliding an external magnet along the device channel. While the assay shows promise in detecting *E. coli*, its detection limit is constrained by the limitations of colorimetric detection (Adkins et al., 2017).

Here, we combine the advantages of magnetophoresis microfluidics and electrochemical techniques for the detection of SARS-CoV-2. To our knowledge, this is the first time the magnetophoretic slider assay (MeSA) has been integrated with electrochemical detection (eMeSA). The eMeSA offers sequential binding of reagents to form a sandwich complex on the magnetic bead, washing away unbound species, and conducting electrochemical measurements, all within a single device at room temperature. Nucleocapsid protein (NP) was chosen as the target analyte since the number of NP in SARS-CoV-2 is greater than the others (the ratio number of N:S protein is 100:1 (Bar-On et al., 2020)), leading to better sensitivity for quantifying the virus. The developed device was successfully applied to detect SARS-CoV-2 NP in 15 nasal swab samples within 10 min after the sample addition containing the bead complex. The eMeSA platform described here represents a novel and straightforward approach with promising implications across various applications.

2. Materials and methods

2.1. Reagents and materials

All chemicals were of analytical reagent grade, and solutions were prepared in deionized Milli-Q® water (18.2 MΩ cm). The details of reagents, materials, and solution preparation are provided in Method S1 in Supplementary data.

2.2. SARS-CoV-2 inactivated virus

SARS-CoV-2 isolate USA-WA1/2020 (NR-52281) was obtained from Biodefense and Emerging Infections Research Resources Repository (BEI Resources). The stocks were prepared in BSL-3 containment by growing the virus in Vero-E6 cells in DMEM (Gibco) containing 10% fetal bovine serum (Atlas Biologicals, USA) and 25 mM HEPES (pH 7.5). To inactivate the virus, the viral stocks were thawed, followed by adding 10% Igepal CA-630 to a final concentration of 0.1% at 4 °C for 30 min. The inactivated virus (IV) was stored at −80 °C and verified for lack of infectivity by plaque assay before being removed from BSL-3 containment. After the viruses were inactivated, the experiment was performed in a BSL-2 biosafety cabinet. To prepare the stock solution, the inactivated virus was diluted using 0.1 M Tris-buffered saline (pH 7.4) with 0.1% (v/v) Tween 20 (TBST) before analysis using static and eMeSA assays.

2.3. Human nasal swab samples

Nasal swab samples were banked samples collected by the staff in Colorado long-term care facilities as part of ongoing surveillance during the pandemic. The process of nasal swab collection is described in Method S2. For static electrochemical and eMeSA assays, 200 μL of the sample was mixed with 400 μL of TBST in a 2-mL microcentrifuge tube, followed by vortexing prior to the initiation of the immunomagnetic separation (IMS) process.

2.4. eMeSA device design and fabrication

The device was designed using CorelDRAW (Corel, Ontario, Canada) and cut using a CO_2 laser cutter (Zing 10000, Epilog Laser). PET transparency film (99 μm thick, 9984, 3M, USA) and double-sided adhesive (120 μm thick, 468 DSA, 3M, USA) were used to create multi-layer channels. As shown in Fig. 1a, the device comprises seven alternating layers of transparency film and DSA (see dimension in Fig. S1). During the fabrication process, the microfluidic channels (L1 - L6) were cut and assembled in a CO_2 laser cutter. The channel geometry in the eMeSA device (*e.g.,* channel heights) was created by optimizing the laser parameters. The conjugated HRP-Ab (8 mm diameter) and TMB pads (3 mm × 5 mm) were inserted into the device between layers L6 and L7 before being covered with the final transparency film layer. The preparation of these two reagent pads is described in Method S3. The cover layer was cut to create the sample inlet and vent holes, while a circular hole was cut in the bottom layer to create the electrochemical detection zone. Subsequently, a commercial screen-printed carbon electrode (4 mm diameter, SPCE, DropSens, Spain) was attached to the bottom layer of the device. Devices were assembled in sets of four before being individually cut for running the assay and kept protected from light until the measurements were performed. The photograph of the eMeSA device after assembly and incorporation of the commercial SPCE is shown in Fig. 1b.

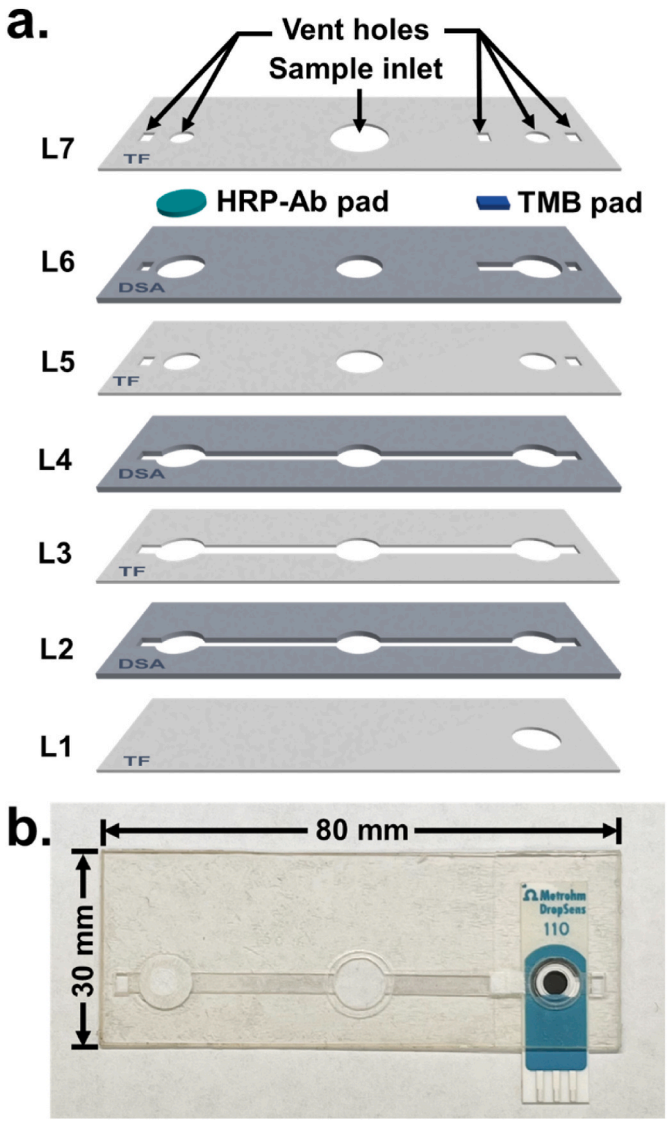

Fig. 1. (a) Exploded view and (b) photograph of the eMeSA device after assembly and incorporation with commercial screen-printed carbon electrode. Note: TF: Transparency film layer; DSA: Double-sided adhesive layer.

2.5. Electrochemical immunoassay for SARS-CoV-2 detection

2.5.1. Static sandwich immunoassay protocol

The immunomagnetic separation (IMS) process of sequential conjugation of the magnetic complex is shown in Fig. S2a, following the supplier protocol with modifications. All steps were performed at room temperature. First, the prepared streptavidin-labeled magnetic beads stock solution was vortexed for 30 s before use (see Method S4 for details on the preparation of the bead stock solution). 20 μL of the beads were added to conjugate to 5 μg/mL of biotinylated Ab and 200 μL of SARS-CoV-2 NP in a microcentrifuge tube for 2.5 min on a rotator. Next, an immunomagnetic separation was performed by washing twice with TBST and using a DynaMag magnet stand to isolate and concentrate the magnetic bead-antibody-antigen complex. After removing the supernatant, 200 μL of 1.25 μg/mL HRP-Ab was added into a microcentrifuge tube to conjugate to the bead complex for 7.5 min on a rotator. The final complex was then washed twice in the presence of a magnet using TBST to remove the unbound species. Finally, the magnetic sandwich complex was resuspended in 50 μL of TBST and stored at 4 °C before use.

Before static assay measurement, the magnetic bead sandwich complex was vortexed for 10 s. Next, 10 μL of the complex was loaded onto the working electrode and magnetically concentrated onto the surface through the magnet positioned just underneath the working electrode (see Fig. S2b). After incubation for 30 s, the residual solution was removed from the working electrode with a pipette. 25 μL of TMB was immediately loaded onto the electrode area and incubated for 2 min. Following the TMB incubation, the magnet was removed, and a chronoamperometric measurement was then performed using a potentiostat (PalmSens 4, Houten, The Netherlands). The potential was held at 0.0 V (*vs.* Ag reference electrode) for 2 min while the reduction current was recorded. The average current signal between t_{60} s and t_{70} s was measured for data acquisition. A calibration curve was obtained by plotting the Δi signal against the concentration of NP. The Δi signal, where $\Delta i = i_{analyte} - i_{blank}$, was used to plot a calibration against the concentration of NP or inactivated virus. The signal-to-noise (S/N) ratio was calculated using the formula $S/N = (i_{analyte} - i_{blank})/i_{blank}$.

2.5.2. eMeSA operation

To perform the assay, the sequential binding of MB/biotinylated Ab/NP complex was first conjugated in a microcentrifuge tube for 2.5 min, as shown in Fig. S3. The complex was then finally resuspended in 50 μL of 1x stable peroxide buffer (SPB, pH 7.4).

The procedure for detecting NP using an eMeSA device is illustrated in Fig. 2. 190 μL of 1x SPB was loaded onto the sample inlet, where a magnet was held stationary underneath the device, followed by adding 10 μL of the prepared MB/biotinylated Ab/NP complex. Within the magnetic field the MB complex was held stationary at the sample inlet while simultaneously, the buffer solution flowed *via* capillary action to both ends of the fluidic channel, rehydrating the HRP-Ab and TMB reagent pads. Next, the magnet was slid to the HRP-Ab pad. During the sliding operation, the MB/biotinylated Ab/NP complexes were moved through the filled microfluidic channel to conjugate with HRP-Ab. After incubating for 7.5 min, the magnet was moved back across the device to the electrochemical detection zone. The final sandwich complex was incubated with TMB substrate for 2 min, followed by chronoamperometric measurement with a potential applied at 0.0 V (*vs.* Ag reference electrode) for another 2 min. The average current signal between t_{60} s and t_{70} s was measured and the Δi signal was used to plot a calibration against the concentration of NP or inactivated virus.

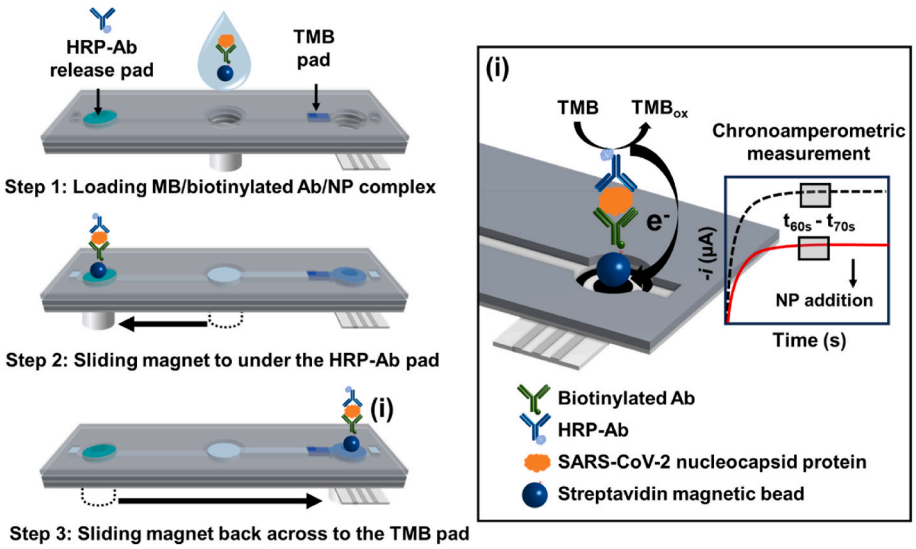

Fig. 2. eMeSA operation for SARS-CoV-2 detection. The assay consists of three steps: (1) Sample addition and rehydration of the reagent pads; (2) magnetic beads are moved from the inlet to beneath the HRP-Ab reagent pad; (3) magnetic beads with the sandwich complexes are moved to the electrochemical detection zone by sliding the magnet across the device. (i) Schematic representation of the electrochemical reaction involved in the eMeSA device responsible for signal generation.

3. Results and discussion

3.1. Detection and mechanism of static SARS-CoV-2 sandwich immunoassay

In this work, the ability to detect the SARS-CoV-2 NP was first demonstrated using a static electrochemical immunoassay. The process described involves conjugating the streptavidin-labeled magnetic bead/biotinylated Ab/NP/HRP-Ab sandwich complex *via* an immunomagnetic separation (IMS). Following the IMS process (see Fig. S2), the bead sandwich complexes containing target NP were preconcentrated on the surface of the working electrode with the magnet located under the working electrode. After removing the supernatant, TMB was loaded onto the electrode. The HRP enzyme then catalyzes the oxidation of TMB

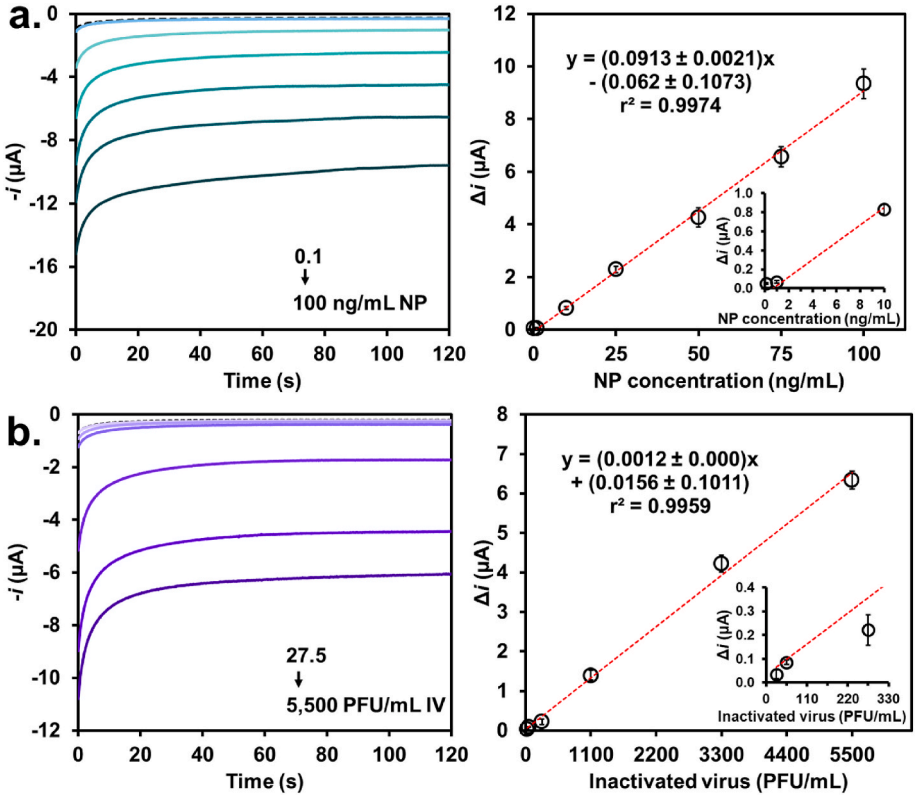

Fig. 3. Representative chronoamperograms for varying concentrations of (a, left) NP in TBST (pH 7.4) and (b, left) inactivated SARS-CoV-2 virus, taken on SPCE using the static electrochemical detection method. Potential was held constant at 0.0 V *vs.* Ag reference for 2 min. The corresponding dose-response curve ranging from (a, right) 0.1–100 ng/mL for the NP and (b, right)27.5 to 5500 PFU/mL for the inactivated virus (n = 4), respectively. Inset: 0.1–10 ng/mL for the NP and 27.5 to 330 PFU/mL for the IV.

when the full sandwich is complete. Subsequently, a 0.0 V potential was applied, resulting in TMB reduction. The solid lines in Fig. 3a are representative chronoamperograms showing the recorded current signals over time during the reduction process of TMB for NP standards and the reagent blank (dotted line). These chronoamperograms show that the reduction current signal approaches a plateau value at 60 s. Therefore, the average current at the time intervals of 60–70 s was used for data acquisition. Besides, the results in Fig. 3a and b clearly show that the current increment is proportional to the NP concentration and inactivated SARS-CoV-2 virus, indicating that the sandwich complex has effectively formed on the magnetic beads.

3.1.1. Static assay optimization

3.1.1.1. Buffer pH. In this work, Tris-buffered saline was used since it is suitable for most biological applications (Biological buffers). 0.1 M Tris-buffered saline with 0.1% (v/v) Tween 20 at pH 7.4 was selected as the binding and washing solution for the whole IMS process (see Fig. S4a and the details of optimization in Supplementary data).

3.1.1.2. Biotinylated Ab concentration and incubation time. Due to the high binding affinity between biotin and streptavidin magnetic beads (Pierce™ Streptavidin Magnetic Beads), a biotinylated antibody was chosen as the capture antibody. This characteristic allows for strong and stable attachment of biotinylated capture antibodies onto the bead surface, ensuring effective immobilization and subsequent recognition of target analytes. Therefore, determining the optimal concentration and incubation time of the biotinylated antibody is essential for effective binding with both the bead and the NP target.

To investigate the effect of biotinylated Ab incubation time on the current signal, 5 μg/mL of biotinylated Ab was conjugated to the beads and NP for 1.0, 2.5, 5.0, 15.0, and 30.0 min, respectively. Fig. S4b shows that at 1.0 min there is no difference in the current in the absence and presence of 10 ng/mL NP. The change of the current becomes evident as a function of the NP concentration when biotinylated Ab was incubated with the beads and NP from 2.5 to 15 min. On the other hand, for 30 min incubation, the current drastically decreased at high antigen concentration (100 ng/mL NP). This phenomenon can be best explained by the Hook effect (Ross et al., 2020). As a result of antigen excess, no sandwich complex can be formed since free antigen competes with captured antigen for detection antibody binding. To achieve good sensitivity and rapid analysis time, 2.5 min was thus selected.

The impact of biotinylated Ab concentration on the current signal was subsequently investigated by testing five different concentrations of biotinylated antibody. As shown in Fig. S4c, the current signals increase with increasing biotinylated Ab concentrations up to 5.0 μg/mL. It was found that 2.5 μg/mL of biotinylated Ab was not a sufficient concentration for capturing NP present in the sample, resulting in saturation of the current signal. The high concentrations of biotinylated Ab, such as 7.5 and 10.0 μg/mL, are not useful as the excess of antibodies could potentially block the electrode surface, hinder the electron transfer, and lead to a decrease in current signals. To achieve high signal noise (S/N) ratios and lower RSDs, 5.0 μg/mL of biotinylated Ab was selected for further study.

3.1.1.3. HRP-Ab concentration and incubation time. HRP-Ab plays an essential role in binding to the target NP and producing a quantifiable signal. HRP is a well-known enzymatic label and is commonly used to label target analytes in traditional ELISAs. With its high turnover rate, affordability, stability, and commercial availability, HRP is an ideal enzyme for point-of-care diagnostics (Sankar et al., 2024; Overview of Detection Probes; Krainer and Glieder, 2015). Figs. S4d and S4e show that the optimal HRP-Ab concentration and incubation time were 1.25 μg/mL HRP-Ab and 7.5 min, respectively. The details of the optimization are provided in the Supplementary data.

3.1.2. Analytical performance for SARS-CoV-2 detection

Using the optimized operating conditions (see Table S1), the magnetoimmunoassay's performance was evaluated for different concentrations of NP diluted in TBST. The results in Fig. 3a show that the calibration was linear in the range of 0.1–100 ng/mL NP, with a linear equation of $(0.913 \pm 0.0021)x - (0.062 \pm 0.1073)$ and coefficient of determination (r^2) of 0.9974. The limit of detection (LOD), defined as a theoretical blank plus 3SD of the blank, was found to be 1.0 ng/mL NP. The RSDs were between 2.4 and 8.0%, in an acceptable range for immunoassays. Our developed static method is sensitive and can detect NP in the concentration range lower than most methods previously reported in the literature. Additionally, the inter-day precision (or repeatability) was evaluated by performing the same static magnetoimmunoassay procedure on five different days. The results in Fig. S5 show that the developed assay provides good inter-day precision (%RSD = 7.5, n = 5 days), with no significant difference in the sensitivities of NP detection across these five days of experiments.

As the end goal of our assay is to detect active viral infection, the concentrations are commonly reported in terms of equivalent plaque-forming units (PFU/mL), which reflects the number of viral particles capable of causing infection. Therefore, the calibration curve for the inactivated virus was then determined. As shown in Fig. 3b, a clear difference can be seen in the current response for varying concentrations of inactivated SARS-CoV-2 virus. The calibration curve, depicted in Fig. 3b, demonstrates a concentration-dependent signal for concentrations ranging from 27.5 to 5500 PFU/mL (linear equation: $0.0012 \pm 0.000)x + (0.0156 \pm 0.1011)$; $r^2 = 0.9959$), with LOD of 10.3 PFU/mL. The RSDs were between 3.3% and 15.4% (n = 32). It is worth noting that this calculated LOD is lower than that of most commercially available rapid antigen tests, typically reported in the 80 to 500 PFU/mL (Cubas-Atienzar et al., 2021; Corman et al., 2021).

3.2. Magnetophoretic slider assay for SARS-CoV-2 detection

Although the static electrochemical immunoassay effectively validates sensing mechanisms, its reliance on multiple pipetting and washing steps makes the process labor-intensive and difficult for all but the most highly trained end-users. In response to these challenges, we have developed an immunosensor that integrates off-device steps from the magnetic bead-based static assay into a microfluidic device known as the magnetophoretic slider assay (MeSA). This advancement aims to simplify processes, reduce the need for user manipulation, and decrease dependence on trained personnel.

The eMeSA device, shown in Fig. 1, is employed to detect SARS-CoV-2 NP. MB/biotinylated Ab is mixed with the sample to provide fast, efficient analyte capture. Next, upon introducing the MB/biotinylated Ab/NP complex into the sample inlet, the bead complex can be easily manipulated within the device by moving an external magnet along the device channel to the desired position. Initially, the MB/biotinylated Ab/NP complex and magnet were moved to the reservoir under the HRP-Ab pad to allow for most contact between the beads and the HRP-Ab, forming sandwich complexes. These complexes are subsequently moved back across the device to the electrochemical detection zone, where they encounter hydrated TMB. TMB undergoes oxidation in the presence of HRP and peroxide when NP is present, followed by reduction due to the voltage applied to the working electrode. Given the short times of the experiments, diffusional mixing of individual components does not occur over the cm length scales of the channels. The resulting reduction current is proportional to the NP concentration in the sample, enabling the quantitative detection of SARS-CoV-2.

3.2.1. eMeSA optimization

In the eMeSA operation, a stable peroxide buffer (SPB, pH 7.4) was utilized because it contains a surfactant that lyses the virus to release the NP from the viral particle along with H_2O_2, which is necessary for the enzymatic reaction between HRP and TMB. Therefore, we investigated

the effect of SPB concentration on the current signal by varying the SPB concentration from 0.5x to 1.5x relative to the concentration provided by the manufacturer. The current signals for 50 ng/mL NP were not significantly impacted by SPB concentrations, unlike the blank (Fig. 4a). Additionally, 1x SPB yielded the highest S/N ratio (1.00 compared to 0.57 and 0.12 for 0.5x and 1.5x SPB, respectively) and was thus chosen for subsequent studies.

The streptavidin magnetic bead is essential for the efficient loading of capture antibodies. As expected, the results in Fig. 4b show that Δi of 50 ng/mL NP significantly increases with the bead mass from 0.01 to 0.02 mg, reaching a plateau at 0.1 mg. Notably, the blank signal also increases slightly with the number of streptavidin magnetic beads, possibly due to the nonspecific adsorption of non-target molecules to the surface of the beads. To reduce nonspecific adsorption, maintain a high S/N ratio, and minimize bead consumption, 0.02 mg of magnetic beads was chosen as an optimal condition.

The next aspect explored was HRP-Ab incubation time and concentration, and the current signals for 50 ng/mL NP increase with increasing HRP-Ab incubation time up to 10 min (Fig. 4c). The blank signal also increases with incubation time, likely due to nonspecific adsorption of HRP-Ab to the bead surface. Additionally, a high S/N ratio and good precision were observed when HRP-Ab was incubated for 7.5 min and thus used for all subsequent experiments. The effect of HRP-Ab concentration was also investigated by varying the concentration loaded on the glass fiber pad from 10 to 20 μg/mL, as shown in Fig. 4b. It was determined that 20 μg/mL of HRP-Ab provided a concentration-dependent signal.

The volume of TMB loaded onto the glass fiber pad was evaluated next. The results in Fig. 4e show that increasing the volume of TMB from 15 to 37.5 μL slightly increases the current. The Δi remains constant when increasing the TMB volume from 30.0 to 37.5 μL. As a result, 30.0 μL of TMB was selected as the optimal volume. Finally, TMB incubation time was investigated. Fig. 4f shows that only 2 min incubation is sufficient to achieve good signal separation between blank and 50 ng/mL NP. Table S2 summarizes the optimal reagents used, their concentration, and incubation time for eMeSA.

3.2.2. Dose-response curves using eMeSA device

The performance of the eMeSA immunosensor in quantifying NP was first evaluated using seven concentrations of NP standards diluted in TBST (0–100 ng/mL NP). Each concentration was tested with four different eMeSA devices (n = 4). The resulting dose-response curve in Fig. 5a shows an increase in current with increasing NP concentration. The data were fitted to a 4 PL curve, and a limit of detection of 8.89 ng/mL NP was calculated using the theoretical blank plus 3SD of the blank. RSDs lower than 8.3% were achieved (0–100 ng/mL NP, n = 28). The eMeSA device was further employed to quantify inactivated SARS-CoV-2 virus. Fig. 5b shows a concentration-dependent signal across 55 to 4400 PFU/mL of inactivated virus, with an LOD of 78.02 PFU/mL. RSDs ranged from 4.4% to 11.9% (n = 32). The concentration range and LOD are sufficient for the broad concentration spectrum found in most COVID-19 cases, which ranges from 5 to 10^6 equivalent PFU/mL (Lin et al., 2022).

3.2.3. Comparison with other magnetic bead-based electrochemical immunoassays

A comparison of our proposed methods with four other magnetic bead-based electrochemical immunoassays is summarized in Table S3. All these methods employed magnetic beads as support for either sandwich-type (Fabiani et al., 2021, 2024; Vásquez et al., 2022) or non-sandwich-type (Malla et al., 2022) immunoassays and utilized a screen-printed electrode as the measurement platform. Methods A (Vásquez et al., 2022) and B (Malla et al., 2022) were developed for S protein detection. These methods provided a low limit of detection. However, they required long assay times and needed to be performed at specific temperature conditions (*e.g.,* incubation at 37 °C and 4 °C for Methods A and B, respectively). Method C (Fabiani et al., 2021) proposed two procedures for S and N proteins using the sandwich assay approach. After performing a sandwich immunoassay, the beads containing the target antigen were preconcentrated on the surface of a carbon black-based SPE, followed by adding 1-naphthyl phosphate as an enzymatic substrate. Enzymatic by-product 1-naphthol was measured by using differential pulse voltammetry (DPV). This immunoassay can be performed at room temperature, providing low LOD and rapid

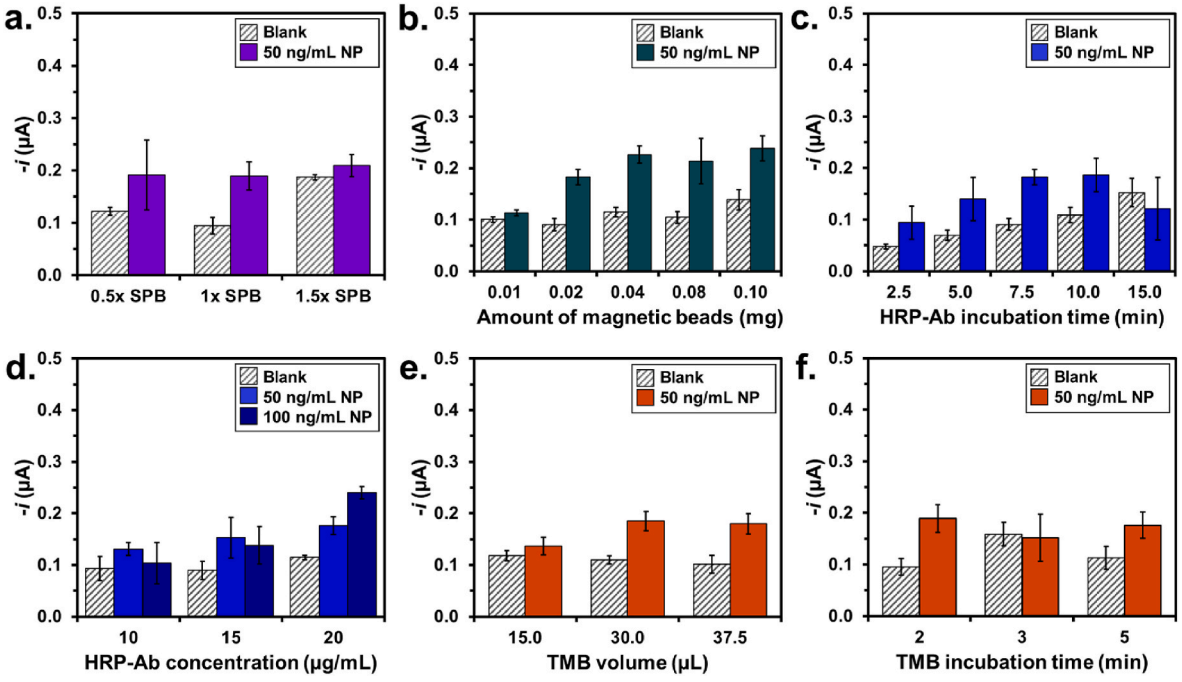

Fig. 4. eMeSA experimental parameter optimization; (a) SPB concentration, (b) amount of streptavidin magnetic beads, (c) HRP-Ab incubation time, (d) HRP-Ab concentration, (e) TMB volume and (f) TMB incubation time. Error bars indicate standard deviation (n = 4).

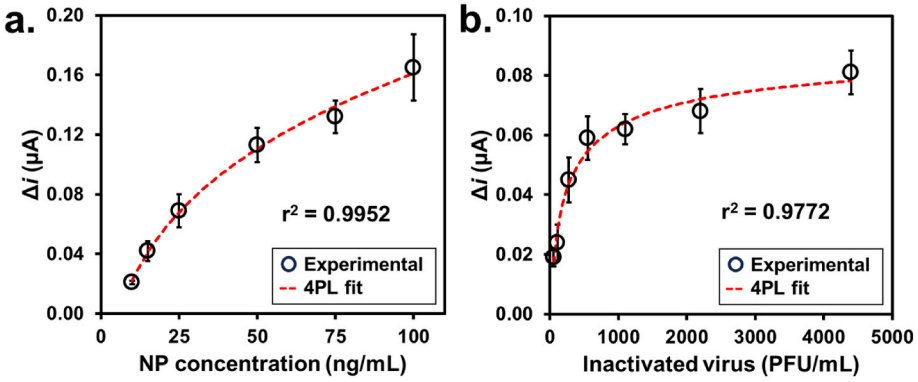

Fig. 5. The dose-response curve of (a) NP in TBST (pH 7.4) and (b) inactivated SARS-CoV-2 virus using the eMeSA device (n = 4). The empirical data for both curves were fitted to 4-parameter logistic curves.

analysis (~30 min). However, the process requires multiple washing steps for both S and N protein assays, which results in significant chemical consumption and waste generation. Method D (Fabiani et al., 2024) employs a magnetic bead-based sandwich immunoassay in conjunction with a paper-based lateral flow device for detecting NP. The lateral flow holder comprises a carbon black-modified SPE with a magnet under the electrode and adsorbent pad. This lateral flow holder is used to manage and minimize waste production. The saliva sample is mixed with all necessary reagents to form a magnetic bead immuno-sandwich complex in the test tube. The prepared solution was added to the device through the hole located over the working electrode, followed by the addition of washing buffer and TMB solution. Despite its ease of use, the challenge with this device is the analysis of glue-like saliva samples, as the high density of saliva can affect the measurement (Yaghmoori et al., 2022).

As shown in Table S3, our method (Method E) achieves a comparable limit of detection with a shorter assay time (compared with the time of at least 135 (Vásquez et al., 2022), 265 (Malla et al., 2022) and 30 (Fabiani et al., 2021, 2024) min). Methods A and B require specific temperature conditions for some incubation steps, whereas the present method is carried out at room temperature (25 °C). The advantages of our eMeSA enable sequential binding of reagents to form a SARS-CoV-2 sandwich complex on the magnetic bead, washing of unbound species, and conducting electrochemical measurements, all within a single device. As a proof of concept, the eMeSA device simplifies the process of conducting static assay by reducing the need for washing and multiple pipetting steps. This not only lowers chemical consumption and waste generation but also shortens the assay time required for static assay to approximately 10 min.

3.2.4. Application in human nasal swab samples

After testing the eMeSA device using lab-prepared inactivated SARS-CoV-2 spiked buffers, the ability to detect NP in human nasal swab samples was assessed. Given the complexity of the biological matrices involved, a sample dilution study was performed to optimize the sample preparation process and ensure accurate and reliable detection. For this purpose, the inactivated SARS-CoV-2 virus stock solution was spiked into the buffer at different VTM:TBST volume ratios to achieve a concentration of 2200 PFU/mL. The results in Fig. S6 show that the more the sample is diluted, the lower the blank signal. The current magnitude of the spiked 2200 PFU/mL inactivated virus was similar across different VTM: TBST volume ratios. Thus, a 1:2 dilution was chosen to provide better signal separation between the blank and the spiked inactivated virus and lower RSDs.

Fifteen samples were collected and analyzed beforehand with RT-qPCR to identify them as positive and negative for SARS-CoV-2 (see C_t value information in Table S4). Each sample was assigned a number and labeled with a plus (+) or minus (−) sign to denote positive or negative results. As shown in Fig. 6, 100% clinical sensitivity and specificity were achieved (Sankar et al., 2024), as all positive samples produced signals above the average control signal, and none of the negative samples provided false positive results. The assay successfully detected SARS-CoV-2 with a C_t value up to 30.3, showing great promise in detecting NP in complex biological matrices. It is crucial to note that the eMeSA device successfully identified positive samples with C_t values exceeding 25, thereby satisfying the World Health Organization's standards for the analytical sensitivity of point-of-care COVID-19 diagnostic tests (WHO). This validates its potential as a reliable and alternative diagnostic tool for identifying SARS-CoV-2 infections.

4. Conclusions

The rapid spread of COVID-19 has highlighted the critical need for developing POC diagnostic tools for multiple pathogens. Here, we have developed, for the first time, a magnetophoretic slider assay with electrochemical detection for POC diagnostics. This approach shows promising results in detecting SARS-CoV-2 with a limit of detection of 8.89 ng/mL NP and 78.02 PFU/mL inactivated virus. eMeSA was used to analyze human nasal swab samples to exhibit 100% clinical sensitivity and specificity compared to RT-PCR results. eMeSA offers an alternative to conventional diagnostic tools by significantly reducing the time required for traditional sandwich ELISA, eliminating the need for

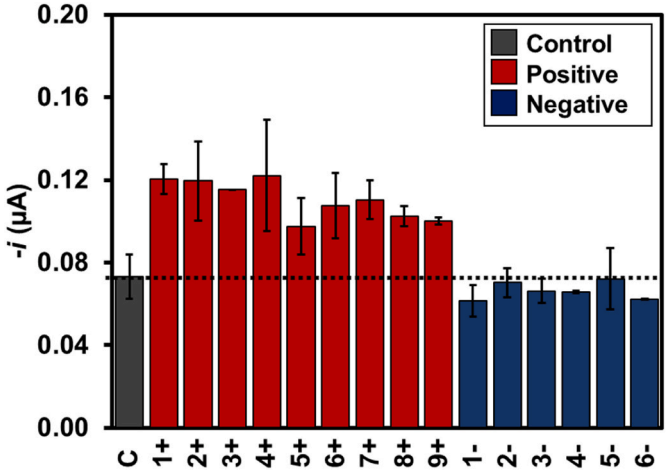

Fig. 6. Analysis of nasal swab patient samples using the eMeSA device, showing the current magnitude of each measurement. C, +, and – signs indicate control (1:2 mixture of virus transfer media and TBST), positive, and negative samples, respectively. Positive and negative samples were indexed with numbers to correlate with the predetermined RT-qPCR cycle threshold (C_t) values in Table S4.

multiple pipetting and washing steps, thereby reducing dependence on trained personnel. Our proposed system could be improved by further integrating sample preparation steps into the MeSA device and testing compatibility with low-cost portable potentiostats. However, due to its simple design and analytical performance being able to identify positive nasal swab samples with C_t value of 30.3, the MeSA has the potential to serve as a versatile tool for rapid disease detection across various healthcare settings.

CRediT authorship contribution statement

Nutnaree Fukana: Writing – review & editing, Writing – original draft, Visualization, Methodology, Investigation, Formal analysis, Conceptualization. **Joowon Park:** Writing – original draft, Investigation, Conceptualization. **Gilberto J. Silva Junior:** Writing – original draft, Methodology. **Lauren E. Malsick:** Methodology. **Emily N. Gallichotte:** Methodology. **Gregory D. Ebel:** Supervision. **Brian J. Geiss:** Writing – review & editing, Resources, Project administration, Methodology, Funding acquisition, Conceptualization. **David S. Dandy:** Writing – review & editing, Resources, Project administration, Methodology, Funding acquisition, Conceptualization. **Mauro Bertotti:** Writing – review & editing, Conceptualization. **Duangjai Nacapricha:** Resources, Project administration, Methodology, Funding acquisition, Conceptualization. **Thaisa A. Baldo:** Writing – review & editing, Writing – original draft, Visualization, Supervision, Investigation, Conceptualization. **Charles S. Henry:** Writing – review & editing, Supervision, Resources, Project administration, Methodology, Conceptualization.

Declaration of competing interest

The authors declare that they have no known competing financial interests or personal relationships that could have appeared to influence the work reported in this paper.

Acknowledgments

This work has been supported by NIH grants (R01 EB031510–01, R01 AI132668, and R61 AI181052) and the São Paulo Research Foundation—FAPESP (2023/00246-1, 2022/09861-8). It is also partially supported by the National Research Council of Thailand: IRN/502/2563 (for DN). The authors would like to thank the scholarships from the Science Achievement Scholarship of Thailand (for NF). The authors acknowledge the support of equipment provided by the Department of Chemistry, Faculty of Science, Colorado State University.

Appendix A. Supplementary data

Supplementary data to this article can be found online at https://doi.org/10.1016/j.bios.2024.117048.

Data availability

Data will be made available on request.

References

Abdelhamid, H.N., Badr, G., 2021. Nanotechnol. Environ. Eng. 6, 19. https://doi.org/10.1007/s41204-021-00109-0.
Adkins, J.A., Boehle, K., Friend, C., Chamberlain, B., Bisha, B., Henry, C.S., 2017. Anal. Chem. 89, 3613–3621. https://doi.org/10.1021/acs.analchem.6b05009.
Afshari, R., Akhavan, O., Hamblin, M.R., Varma, R.S., 2021. ACS Appl. Nano Mater. 4, 11386–11412. https://doi.org/10.1021/acsanm.1c01907.
Akhavan, O., Ghaderi, E., Rahighi, R., 2012. ACS Nano 6, 2904–2916. https://doi.org/10.1021/nn300261t.
Bar-On, Y.M., Flamholz, A., Phillips, R., Milo, R., 2020. Elife 9, e57309. https://doi.org/10.7554/eLife.57309.
Biological buffers: Buferring range, https://www.hopaxfc.com/en/product/category/biological-buffers.
Cajigas, S., Alzate, D., Fernández, M., Muskus, C., Orozco, J., 2022. Talanta 245, 123482. https://doi.org/10.1016/j.talanta.2022.123482.
Call, Z.D., Carrell, C.S., Jang, I., Geiss, B.J., Dandy, D.S., Henry, C.S., 2020. Anal. Methods 12, 5177–5185. https://doi.org/10.1039/D0AY01523G.
Call, Z.D., Dolence, A., Boes, J., Henry, C.S., 2023. Front. Sens. 3. https://doi.org/10.3389/fsens.2022.1080037.
Corman, V.M., Haage, V.C., Bleicker, T., Schmidt, M.L., Mühlemann, B., Zuchowski, M., et al., 2021. The Lancet Microbe 2, e311–e319. https://doi.org/10.1016/S2666-5247(21)00056-2.
Cubas-Atienzar, A.I., Kontogianni, K., Edwards, T., Wooding, D., Buist, K., Thompson, C. R., et al., 2021. Sci. Rep. 11, 18313. https://doi.org/10.1038/s41598-021-97489-9.
Durmus, C., Balaban Hanoglu, S., Harmanci, D., Moulahoum, H., Tok, K., Ghorbanizamani, F., et al., 2022. Talanta 243, 123356. https://doi.org/10.1016/j.talanta.2022.123356.
Fabiani, L., Saroglia, M., Galatà, G., De Santis, R., Fillo, S., Luca, V., et al., 2021. Biosens. Bioelectron. 171, 112686. https://doi.org/10.1016/j.bios.2020.112686.
Fabiani, L., Fiore, L., Fillo, S., D'Amore, N., De Santis, R., Lista, F., et al., 2024. Bioelectrochemistry 156, 108619. https://doi.org/10.1016/j.bioelechem.2023.108619.
Fenwick, C., Croxatto, A., Coste, A.T., Pojer, F., André, C., Pellaton, C., et al., 2021. J. Virol. 95. https://doi.org/10.1128/jvi.01828-20.
Ferreira, M.D., Yamada-Ogatta, S.F., Teixeira Tarley, C.R., 2023. Biosensors 13. https://doi.org/10.3390/bios13030336.
Giri, B., Pandey, S., Shrestha, R., Pokharel, K., Ligler, F.S., Neupane, B.B., 2021. Anal. Bioanal. Chem. 413, 35–48. https://doi.org/10.1007/s00216-020-02889-x.
Kilic, T., Weissleder, R., Lee, H., 2020. iScience 23, 101406. https://doi.org/10.1016/j.isci.2020.101406.
Krainer, F.W., Glieder, A., 2015. Appl. Microbiol. Biotechnol. 99, 1611–1625. https://doi.org/10.1007/s00253-014-6346-7.
Kudr, J., Klejdus, B., Adam, V., Zitka, O., 2018. TrAC, Trends Anal. Chem. 98, 104–113. https://doi.org/10.1016/j.trac.2017.10.023.
Kudr, J., Michalek, P., Ilieva, L., Adam, V., Zitka, O., 2021. TrAC, Trends Anal. Chem. 136, 116192. https://doi.org/10.1016/j.trac.2021.116192.
Kumar, N., Shetti, N.P., Jagannath, S., Aminabhavi, T.M., 2022. Chem. Eng. J. 430, 132966. https://doi.org/10.1016/j.cej.2021.132966.
Lin, Y.-C., Malott, R.J., Ward, L., Kiplagat, L., Pabbaraju, K., Gill, K., et al., 2022. Sci. Rep. 12, 5418. https://doi.org/10.1038/s41598-022-09218-5.
Liu, Y., Zhan, L., Qin, Z., Sackrison, J., Bischof, J.C., 2021. ACS Nano 15, 3593–3611. https://doi.org/10.1021/acsnano.0c10035.
Madhurantakam, S., Muthukumar, S., Prasad, S., 2022. ACS Omega 7, 12467–12473. https://doi.org/10.1021/acsomega.2c00638.
Malla, P., Liao, H.-P., Liu, C.-H., Wu, W.-C., Sreearunothai, P., 2022. Microchim. Acta 189, 168. https://doi.org/10.1007/s00604-022-05288-4.
Malla, P., Liu, C.-H., Wu, W.-C., Kabinsing, P., Sreearunothai, P., 2023. Talanta 262, 124701. https://doi.org/10.1016/j.talanta.2023.124701.
Naghdi, M., Ghovvati, M., Rabiee, N., Ahmadi, S., Abbariki, N., Sojdeh, S., et al., 2022. Adv. Colloid Interface Sci. 308, 102771.
Naorungroj, S., Srisomwat, C., Khamcharoen, W., Jampasa, S., Pasomsub, E., Shin, K., et al., 2023. Anal. Chem. 95, 12794–12801. https://doi.org/10.1021/acs.analchem.3c01758.
Nascimento, E.D., Fonseca, W.T., de Oliveira, T.R., de Correia, C.R.S.T.B., Faça, V.M., de Morais, B.P., et al., 2022. Sens. Actuators, B 353, 131128. https://doi.org/10.1016/j.snb.2021.131128.
Ong, D.S.Y., de Man, S.J., Lindeboom, F.A., Koeleman, J.G.M., 2020. Clin. Microbiol. Infection 26 (1094). https://doi.org/10.1016/j.cmi.2020.05.028 e1097-1094. e1010.
Overview of Detection Probes, https://www.thermofisher.com/th/en/home/life-science/protein-biology/protein-biology-learning-center/protein-biology-resource-library/pierce-protein-methods/overview-detection-probes.html.
Paleček, E., Fojta, M., 2007. Talanta 74, 276–290. https://doi.org/10.1016/j.talanta.2007.08.020.
Pamme, N., Manz, A., 2004. Anal. Chem. 76, 7250–7256. https://doi.org/10.1021/ac049183o.
Perveen, S., Negi, A., Gopalakrishnan, V., Panda, S., Sharma, V., Sharma, R., 2023. Clin. Chim. Acta 538, 139–156. https://doi.org/10.1016/j.cca.2022.11.017.
Pierce™ Streptavidin Magnetic Beads, https://www.thermofisher.com/document-connect/document-connect.html?url= https://assets.thermofisher.com/TFS-Assets/2FLSG/2Fmanuals/2FMAN0011642_Pierce_Streptavidin_Mag_Bead_UG.pdf.
Rad, M., Ebrahimipour, G., Bandehpour, M., Akhavan, O., Yarian, F., 2023. Appl. Phys. A 129, 401. https://doi.org/10.1007/s00339-023-06620-2.
Rahman, M.M., 2022. Chemosensors 10. https://doi.org/10.3390/chemosensors10070287.
Rocha, D.S., Baldo, T.A., Silva-Neto, H.A., Duarte-Junior, G.F., Bazílio, G.S., Borges, C.L., et al., 2024. Talanta 268, 125337. https://doi.org/10.1016/j.talanta.2023.125337.
Ross, G.M.S., Filippini, D., Nielen, M.W.F., Salentijn, G.I.J., 2020. Anal. Chem. 92, 15587–15595. https://doi.org/10.1021/acs.analchem.0c03740.
Sankar, K., Kuzmanović, U., Schaus, S.E., Galagan, J.E., Grinstaff, M.W., 2024. ACS Sens. 9, 2254–2274. https://doi.org/10.1021/acssensors.4c00043.
Vásquez, V., Navas, M.-C., Jaimes, J.A., Orozco, J., 2022. Anal. Chim. Acta 1205, 339718. https://doi.org/10.1016/j.aca.2022.339718.
WHO, COVID-19 Target product profiles for priority diagnostics to support response to the COVID-19 pandemic v.1.0, https://www.who.int/publications/m/item/covid-19-target-product-profiles-for-priority-diagnostics-to-support-response-to-the-covid-19-pandemic-v.0.1.

WHO COVID-19 dashboard, https://data.who.int/dashboards/covid19/deaths?n=o.
Wu, W., Cheng, Y., Zhou, H., Sun, C., Zhang, S., 2023. Virol. J. 20, 6. https://doi.org/10.1186/s12985-023-01968-6.
Yaghmoori, K., Mousavi, E., Khosravi, S., Hatamzade, Z., Ghahremani, N., Amiri, A., Pharm, J., 2022. Negat. Results 13, 1160–1166. https://doi.org/10.47750/pnr.2022.13.04.162.